



Article

Signal Processing Methods of Enhanced Magnetic Memory Testing

Xu Luo ^{1,*}, Lihong Wang ¹ , Shufeng Cao ¹, Qiuhan Xiao ¹ , Hongjuan Yang ¹ and Jianguo Zhao ²¹ School of Mechanical and Electrical Engineering, Chengdu University of Technology, Chengdu 610059, China² School of Mechatronic Engineering, Southwest Petroleum University, Chengdu 610500, China

* Correspondence: luoxu@cdut.edu.cn

Abstract: As a particular kind of detection technology under weak magnetization, metal magnetic memory testing is very likely to be affected by external factors in the detecting process, which may lead to incorrect results. In order to minimize the negative influence of interrupting signals and improve the detection accuracy, this paper adopted the enhanced metal magnetic memory testing method to preliminarily increase the signal-to-noise ratio (SNR) of the detection signal and then compares the denoising effects of wavelet threshold denoising method, empirical mode decomposition (EMD) denoising method, EMD-wavelet threshold denoising method, ensemble EMD (EEMD), complementary EEMD (CEEMD), variational mode decomposition (VMD), local mean decomposition (LMD) and empirical wavelet transform (EWT) on the detection signal and the gradient signal respectively. The results show that the enhanced metal magnetic memory testing method can significantly increase the SNR of the obtained signal and cannot improve the SNR of a gradient signal which is generated from the obtained signal. The different denoising methods can further boost the SNR and improve the detection accuracy of the obtained signal and the gradient signal. Among the eight signal processing methods, wavelet threshold, EMD and its improved methods are more applicable in the denoising of enhanced metal magnetic memory testing signals. The Wavelet threshold denoising, EMD-wavelet threshold denoising and EEMD denoising all have good denoising effects, and the denoising results to the same signal are analogous.

Keywords: enhanced metal magnetic memory testing; signal processing; wavelet threshold denoising; EMD-wavelet threshold denoising; EEMD denoising



Citation: Luo, X.; Wang, L.; Cao, S.; Xiao, Q.; Yang, H.; Zhao, J. Signal Processing Methods of Enhanced Magnetic Memory Testing. *Processes* **2023**, *11*, 302. <https://doi.org/10.3390/pr11020302>

Academic Editor: Jie Zhang

Received: 20 December 2022

Revised: 11 January 2023

Accepted: 12 January 2023

Published: 17 January 2023



Copyright: © 2023 by the authors. Licensee MDPI, Basel, Switzerland. This article is an open access article distributed under the terms and conditions of the Creative Commons Attribution (CC BY) license (<https://creativecommons.org/licenses/by/4.0/>).

1. Introduction

Ferromagnetic materials will inevitably result in early damage, such as stress concentration, microplastic deformation and micro-cracks when they are used. With the accumulation and expansion of early damage, macroscopic volume defects will eventually cause structural failure. To ensure structural safety, it is very important to detect and evaluate the damage to the material [1]. In 1994, Russian scholar Professor Dubov was the first person to propose the metal magnetic memory testing method, which was known as a new non-destructive testing technique of the 21st century [2]. As a magnetic testing technology under weak magnetization, the metal magnetic memory testing signal is weak, and the testing results are susceptible to external disturbing factors. Enhanced metal magnetic memory testing improves the sensitivity and accuracy of detection by applying an appropriate intensity of directional magnetic field to the specimen to minimize interference [3,4]. However, the obtained signal contains a lot of random noise, and consequently, useful information cannot be directly extracted from the signal and the gradient signal. Therefore, to denoise the enhanced metal magnetic memory testing signal and to eliminate the bad effects of the noise on the signal, especially the signal gradient, by using appropriate signal processing methods has great significance for identifying defect feature signals and eigenvalues precisely.

Wang et al. [5], Jian et al. [6] and Zhu et al. [7] applied wavelet transform and adaptive wavelet threshold to denoise the metal magnetic memory testing signal, respectively, which

greatly boosted the SNR of the obtained signal [8,9]. EMD is an adaptive decomposition method that does not include the complicated process of selecting basis functions. It can boost the recognition rate of defects [10–12]. Nevertheless, the endpoint effect and modal mixing of EMD will influence the decomposition accuracy. Based on it, Wu and Huang proposed an improved method of adding noise—EEMD, which can effectively suppress modal mixing [13]. EEMD can be used to remove the noise in the wire rope or pipeline defect detection signal, but the auxiliary white noise added in the decomposition process cannot be eliminated completely [14–16]. CEEMD eliminates the influence of residual auxiliary noise in EEMD by adding paired noise, but it is difficult to align IMF components when ensemble averaging, and the error still exists [17–19]. In addition, VMD, LMD, and EWT are also applied to signal denoising; Ju et al. researched the defect signal extraction algorithm of steel pipeline based on improved VMD [20], Chen et al. performed fault diagnosis of rolling bearing with LMD [21], and Lu et al. denoised microseismic noise based on EWT and Meyer adaptive threshold [22].

Nevertheless, for the noise reduction of magnetic memory detection signals, wavelet threshold denoising and empirical mode decomposition are still the most commonly used. In order to improve the quality of signal denoising, the EMD denoising and wavelet threshold denoising are combined in this paper.

Firstly, this paper analyzes the effect of the enhanced metal magnetic memory testing method on improving the SNRs of obtained signal and the gradient signal. Secondly, this paper uses eight signal processing methods to denoise the obtained signal and analyzes the denoising effects of those signal processing methods on the enhanced metal magnetic memory testing signal. Through the analysis of the denoising results, the most suitable signal processing method for the enhanced metal magnetic memory testing signal is determined.

2. Experimental Design and Signal Sampling

As shown in Figure 1, the subject of the experiment is a Q235 specimen with a length of 200 mm, a width of 40 mm, and a thickness of 3 mm. A rectangular defect with a length of 10 mm, a width of 1 mm, and a depth of 3 mm was present in the center of the specimen. The testing system consists of an excitation device, motion actuator and signal acquisition device. Place the specimen on a stainless steel lifting table, using the U-shaped yoke to magnetize the defect area of the specimen, and the state of the specimen is unsaturated magnetic when the current of the excitation power supply is 0.7A. The magnetic signal of the surface of the specimen is measured by the CH-3600 three-dimensional Gaussian meter. In the process of measurement, the three-axis CNC displacement platform is used to control the movement of the detection probe. The magnetic signal is collected within a scanning area, and this 20 mm × 20 mm area is less than 1 mm from the central surface. There are 40 sampling paths in total. The spacing between paths is 0.5 mm, and each path has 1200 sampling points. The specimen is demagnetized before the experiment to eliminate the influence of mechanical processing on the magnetic signal.

Figure 2 shows the normal component H_x , tangential component H_y , and horizontal component H_z of the metal magnetic memory testing signal and their gradient values in the geomagnetic field. It can be easily seen that the metal magnetic memory testing signal is weak and contains a lot of interference information. Therefore, it is impossible to determine the exact positions of the peak-to-valley value H_x and the maximum value of H_y . Because of the loud noise, it is impossible to receive the defect information in the gradient signal value.

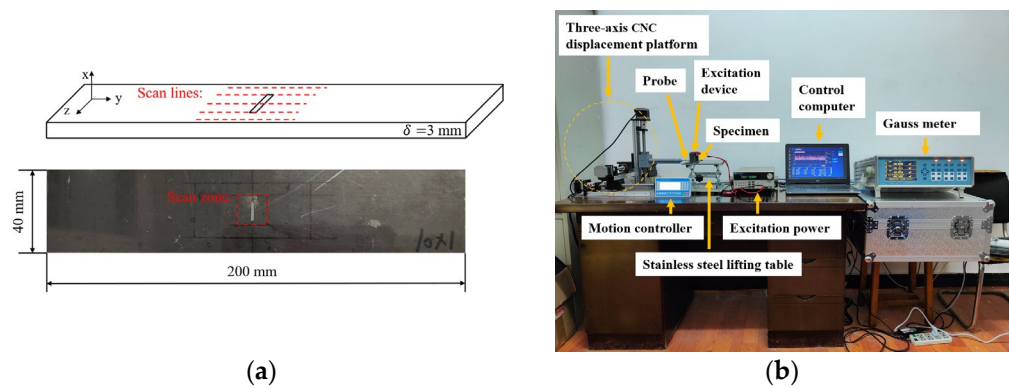


Figure 1. Enhanced metal magnetic memory testing system and specimen diagram. (a) Q235 specimen. (b) Enhanced metal magnetic memory testing system.

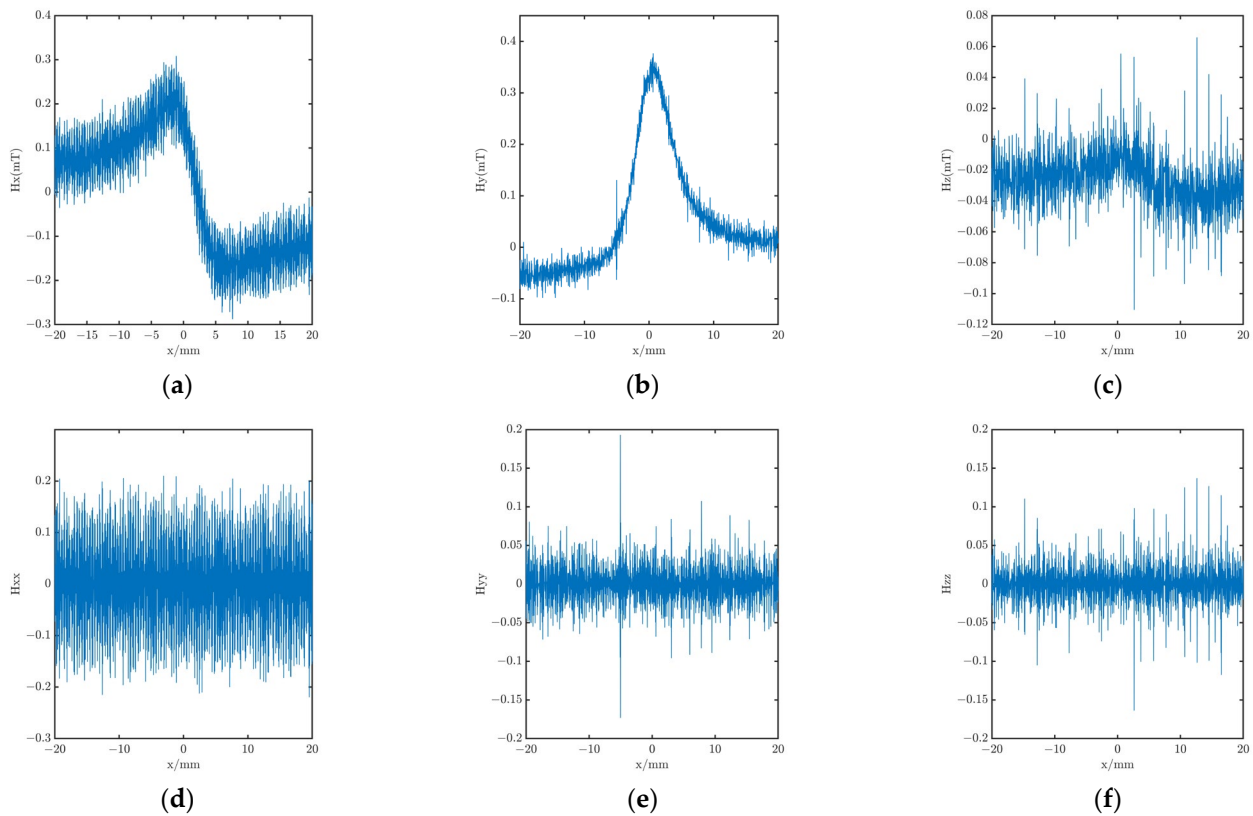


Figure 2. Metal magnetic memory testing signal and magnetic gradient signal. (a) Normal component signal. (b) Tangential component signal. (c) Horizontal component signal. (d) Gradient value of the normal component signal. (e) Gradient value of the tangential component testing signal. (f) Gradient value of the horizontal component testing signal.

In order to improve the detection accuracy, the enhanced metal magnetic memory testing method, which applies a certain intensity of external excitation magnetic field to the specimen, is adopted. The obtained signal components and their gradient signals are shown in Figure 3.

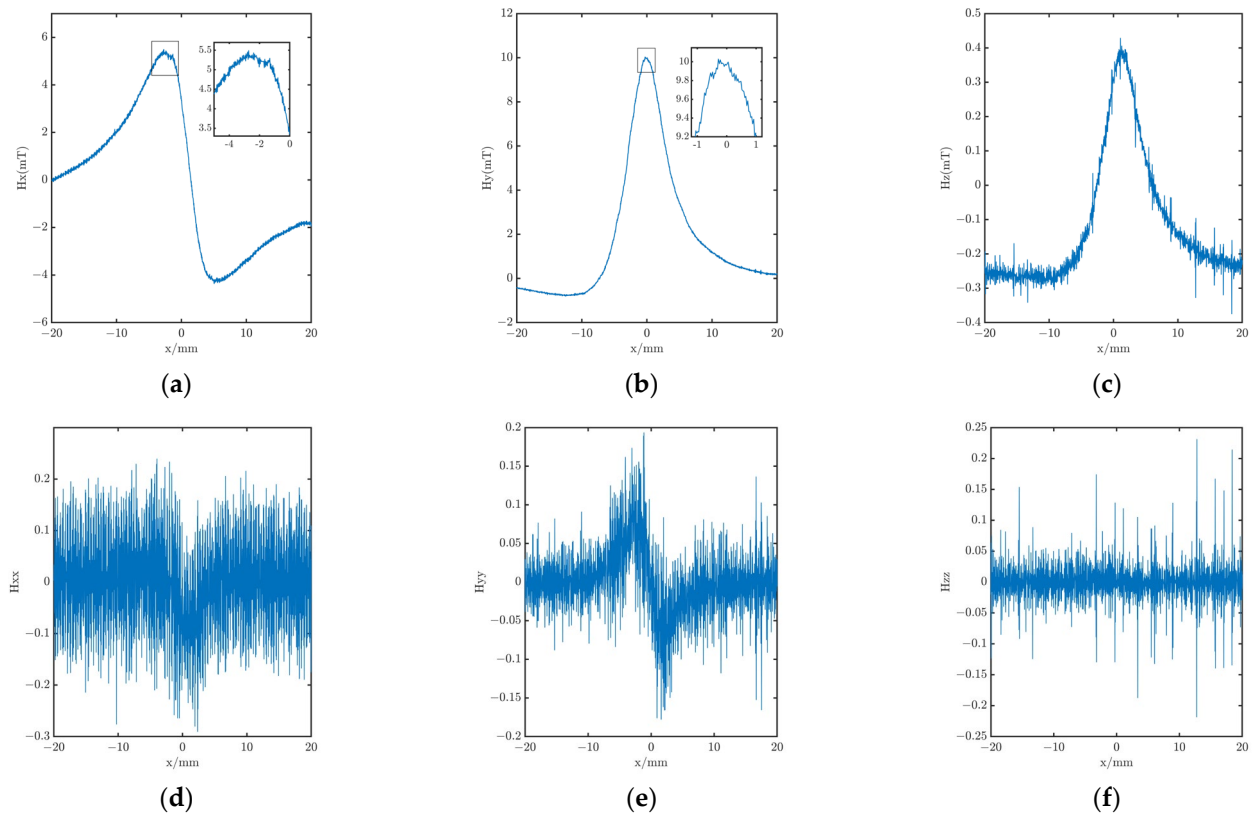


Figure 3. Enhanced metal magnetic memory testing signal and magnetic gradient signal. (a) Normal component signal. (b) Tangential component signal. (c) Horizontal component signal. (d) Gradient value of the normal component signal. (e) Gradient value of the tangential component signal. (f) Gradient value of the horizontal component signal.

It can be seen from Figure 3 that after adopting the external magnetic field properly, the amplitude of each component of the collected magnetic field signal increases, and the signal curve is relatively gentle, which can reflect the defect information better. The curve of H_x passes through the zero point in the center of the defect, and there are peak-to-valley values on the left and right edges of the defect. The H_y and H_z have maximum values at the defect center. The normal component gradient signal H_{xx} and the tangential component gradient signal H_{yy} have roughly demonstrated the top-to-bottom values and extreme values of the defect edge information. These all indicate that the enhanced metal magnetic memory testing method can improve the sensitivity and detection accuracy of defect detection to a certain extent.

However, since the collected signal still contains noise signals, the gradient calculation further amplifies the influence of the noise signal. Thus, the exact position of the extreme point cannot be obtained in the H_{xx} and H_{yy} signal curves. In addition, the information related to the defect in the gradient signal of the horizontal component H_{zz} is still drowned by noise. Therefore, it is necessary to use appropriate signal processing methods to denoise the collected signals so as to better obtain the eigenvalues that can characterize the defects from each component of the magnetic signal and its gradient value.

3. Signal Processing Methods

3.1. Wavelet Threshold Denoising

Wavelet threshold denoising consists of three stages. In Stage One, according to the characteristics of the obtained signal, the appropriate wavelet basis function and decomposition level are selected to decompose the obtained signal. In Stage Two, threshold processing is performed on the wavelet coefficients of each scale obtained by decomposition to remove high-frequency noise. In Stage Three, the processed signals of each scale are

reconstructed to obtain the denoised signal. The selection of wavelet basis function and decomposition level plays a vital role in the whole process.

According to the wavelet basis functions Daubechies, Symlets, and Coiflets used in the literature [6,8,16,23], db2~db10, sym2~sym10 and coif1~coif5 wavelet basis are used to denoise the signal with wavelet soft threshold denoising. Adaptive threshold selection is done on the principle of Stein’s Unbiased Risk Estimate, and with decomposition levels ranging from 4 to 6, the effectiveness of denoising is calculated.

The SNR is utilized to evaluate denoising effectiveness. The larger the SNR is, the better the denoising effectiveness is. The calculation method is shown in Formula (1):

$$SNR = 10 \lg \frac{\frac{1}{N} \sum_{n=1}^N s^2(n)}{\frac{1}{N} \sum_{n=1}^N [s(n) - \hat{s}(n)]^2} \tag{1}$$

where $s(n)$ is the original signal, $\hat{s}(n)$ is the denoised signal, and N is the data length.

Figure 4 shows the denoising effect with different wavelet base functions and at different decomposition levels. It is clear that the signal-denoising effect varies with the different functions and levels.

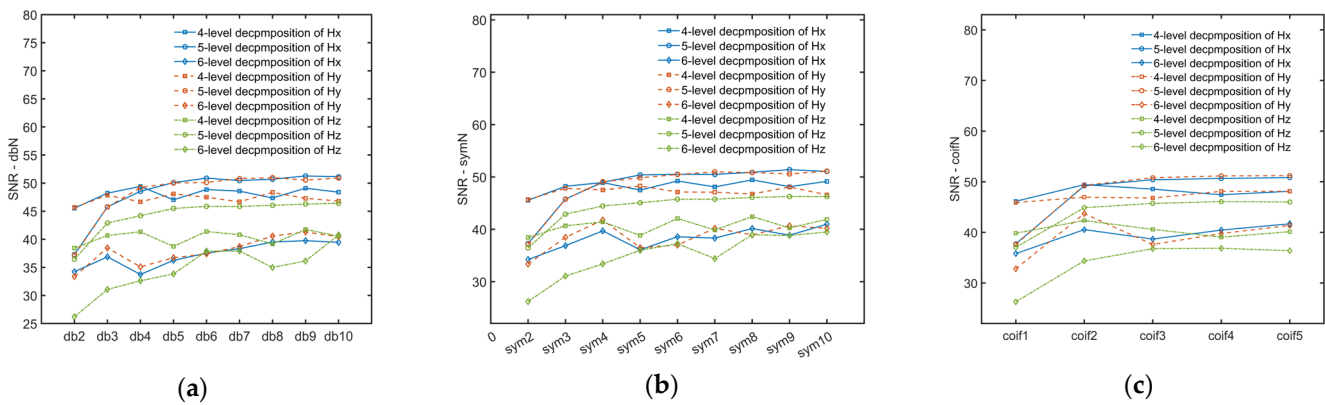


Figure 4. Denoising effect of different wavelet basis functions under different decomposition levels. (a) Denoising effect of dbN. (b) Denoising effect of symN. (c) Denoising effect of coifN.

The three wavelet basis functions all have the best denoising effect when the decomposition level is 5. With the increase of vanishing moment, the SNR first climbs and then becomes stable. The normal component H_x has the highest SNR of 51.3965 in the 5-level decomposition of sym9, the tangential component H_y has the highest SNR of 51.2075 in the 5-level decomposition of coif5, and the horizontal component H_z has the highest SNR of 46.4024 in the 5-level decomposition of db10.

At the highest SNR, the wavelet basis function and the number of decomposition layers are used to denoise the signal, respectively. The results of each component of the magnetic signal and its gradient value after denoising are shown in Figure 5. It can be seen that the high-frequency noise and instantaneous pulse in the original signal can be removed through wavelet threshold denoising, and the curves of different component signals and their gradient signals become flat, especially the characteristics of gradient signal which are related to defects where the minimum value of H_{xx} is connected with the defect center, and the peak-to-valley value of H_{yy} is connected with the left and right boundaries of the defect. However, in the process of the wavelet transform, the selection of wavelet basis functions and decomposition scales has a great influence on the wavelet denoising effect. When the detection signal changes, the best wavelet basis function and decomposition level must be reselected.

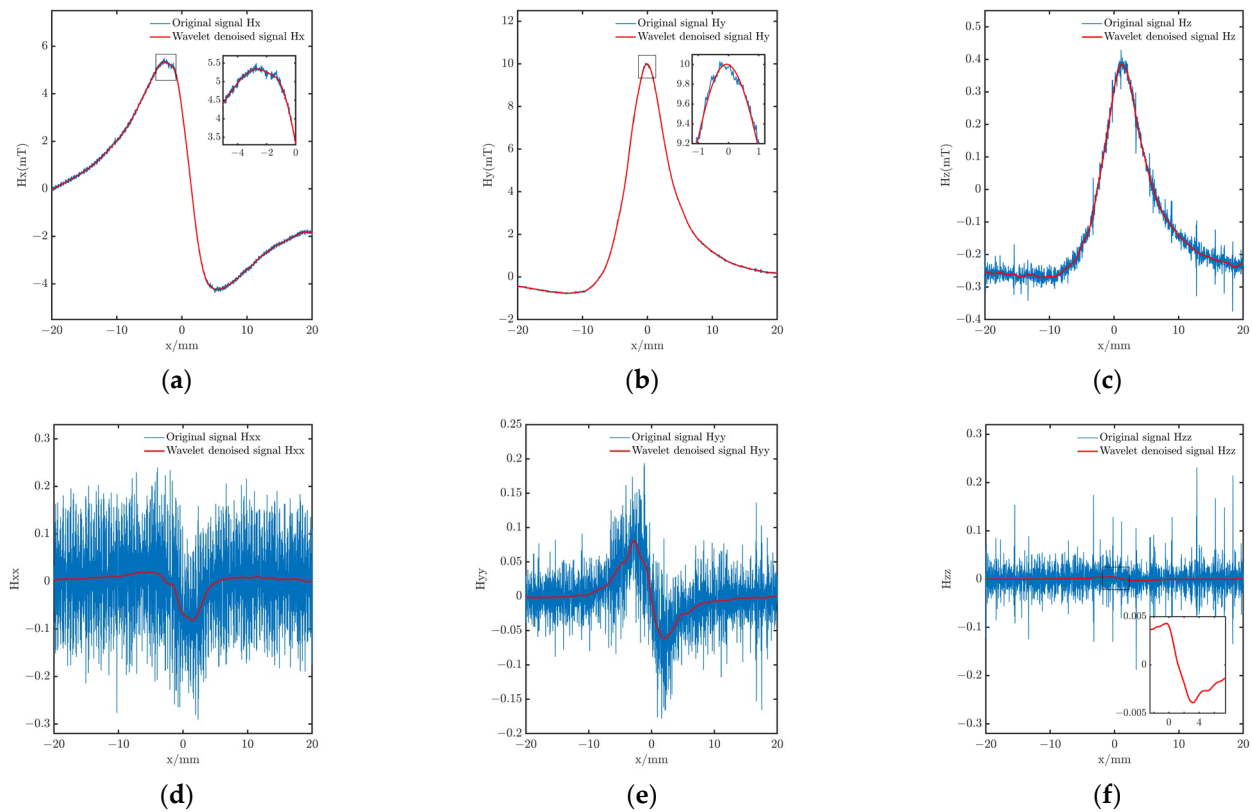


Figure 5. Comparison of wavelet threshold denoising effects. (a) Comparison of normal component signals. (b) Comparison of tangential component signals. (c) Comparison of horizontal component signals. (d) Comparison of gradient values of normal component signal. (e) Comparison of gradient values of tangential component signal. (f) Comparison of gradient values of horizontal component signal.

3.2. EMD Denoising

EMD can deal with non-stationary and nonlinear signals well. According to the time scale characteristics of the signal, EMD performs signal decomposition. This can avoid pre-setting the basis function and is much better than other time domain analysis methods. The signal decomposed by EMD contains several intrinsic mode functions (IMF) and a trend term, which can be recorded as:

$$s(n) = \sum_{k=1}^K \text{IMF}_k(n) + r(n) \quad (2)$$

where $s(n)$ is the original signal; $\text{IMF}_k(n)$ is the k -th IMF component; K is the K -th IMF component obtained by decomposition; and $r(n)$ is the remaining trend term of decomposition.

Figure 6 shows the EMD decomposition diagram of each component of the enhanced metal magnetic memory testing signal. The original signal H_x is decomposed into 9 IMF components and 1 trend term. Among them, IMF 1, IMF 2 and IMF 3 have high frequency and small amplitude, which are judged as high-frequency random noise in the detection process. The IMF 4 component has low frequency and small amplitude, which is judged as lift-off noise or low-frequency noise generated by the detection probe. Therefore, in the EMD denoising process, the IMF 1–IMF 4 components are removed. Then the remaining IMF components and trend term are reconstructed to obtain the normal component signal H_x . Similarly, the high-frequency noise components IMF 1, IMF 2, and the low-frequency noise component IMF 3 of H_y are eliminated, and then the remaining signals are reconstructed to obtain the tangential component signal; the high-frequency noise components IMF 1–IMF 3 and low-frequency noise components IMF 4 and IMF 5 of H_z are

eliminated, and then the remaining components are reconstructed to obtain the horizontal component signal.

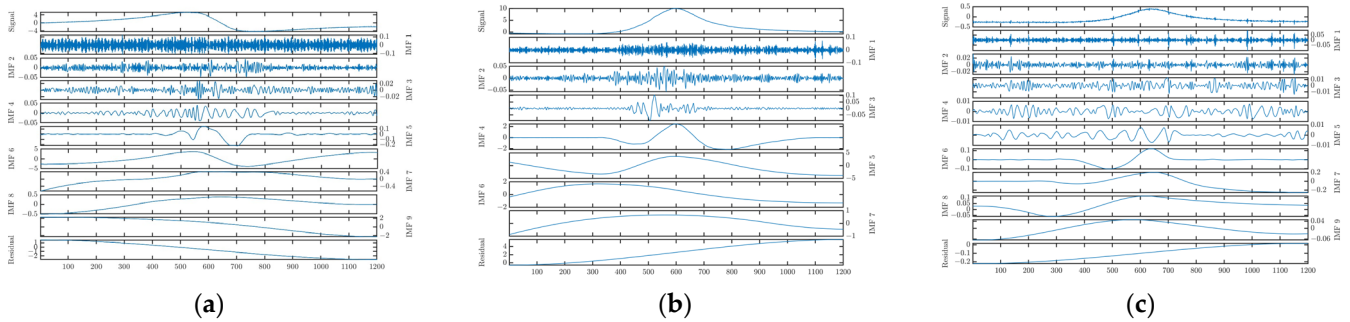


Figure 6. EMD decomposition diagram of enhanced magnetic memory testing signal. (a) EMD decomposition diagram of the normal component. (b) EMD decomposition diagram of the tangential component. (c) EMD decomposition diagram of the horizontal component.

Figure 7 shows the signal components and their gradient values obtained by EMD denoising. It can be seen that the EMD denoising takes away the random noise and strong pulse interference in the processed signal. The defect characteristics of the gradient value of different component signals are obvious, and the left and right boundary positions of the defect can be determined accordingly.

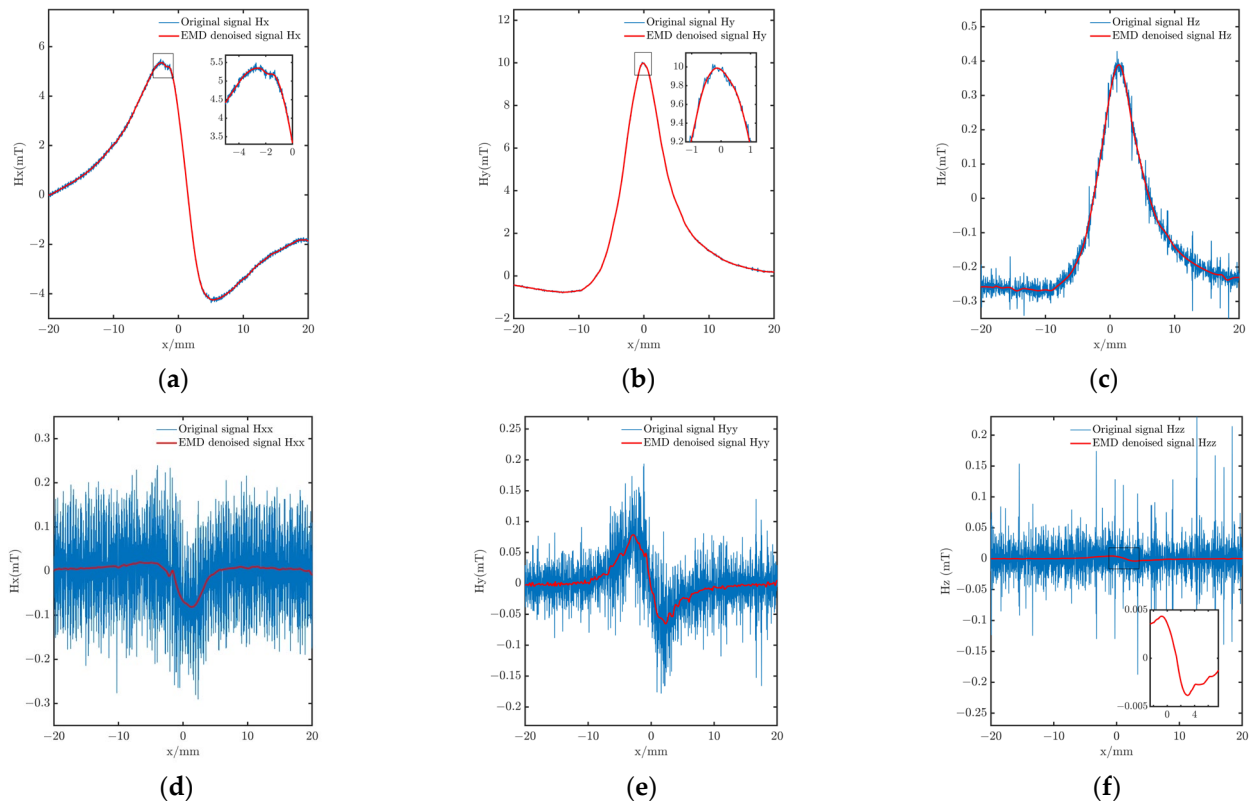


Figure 7. Comparative diagram of EMD denoising effect. (a) Comparison of normal component signals. (b) Comparison of tangential component signals. (c) Comparison of horizontal component signals. (d) Comparison of gradient values of normal component signal. (e) Comparison of gradient values of tangential component signal. (f) Comparison of gradient values of horizontal component signal.

3.3. EMD-Wavelet Threshold Denoising

Through the above analysis, it can be proven that the wavelet threshold denoising method and EMD denoising method can both greatly improve the SNR of obtained signal. Consequently, the EMD denoising and wavelet threshold denoising are combined. The combined EMD-wavelet threshold denoising method is employed to process the enhanced metal magnetic memory signal, and then the denoising result of the combined method is analyzed. The general process is shown in Figure 8, and the steps are as follows.

1. Decompose signals into several IMF components and a trend term by EMD;
2. Calculate the correlation coefficient R of each order IMFs respectively, and the calculation method is shown in Formula (3). If the order of the first local minimum value of R is j , then IMF_{j+1} is the transitional component of noise and useful signal;
3. The high-frequency signal before IMF_{j+1} is processed by the soft threshold and then reconstructed the signal with the other IMF components and trend item;
4. With the same number of decomposition layers and the same scale as mentioned earlier in this paper, the reconstructed signal is processed by wavelet threshold to obtain the denoised signal.

$$R = \frac{\sum_{n=1}^N [s(n) - \bar{s}(n)] [IMF_k(n) - \overline{IMF_k}(n)]}{\sqrt{\sum_{n=1}^N [s(n) - \bar{s}(n)]^2} \sqrt{\sum_{n=1}^N [IMF_k(n) - \overline{IMF_k}(n)]^2}} \quad (3)$$

where $IMF_k(n)$ is the k -th IMF component, and $\overline{IMF_k}(n)$ is the mean of the k -th IMF component.

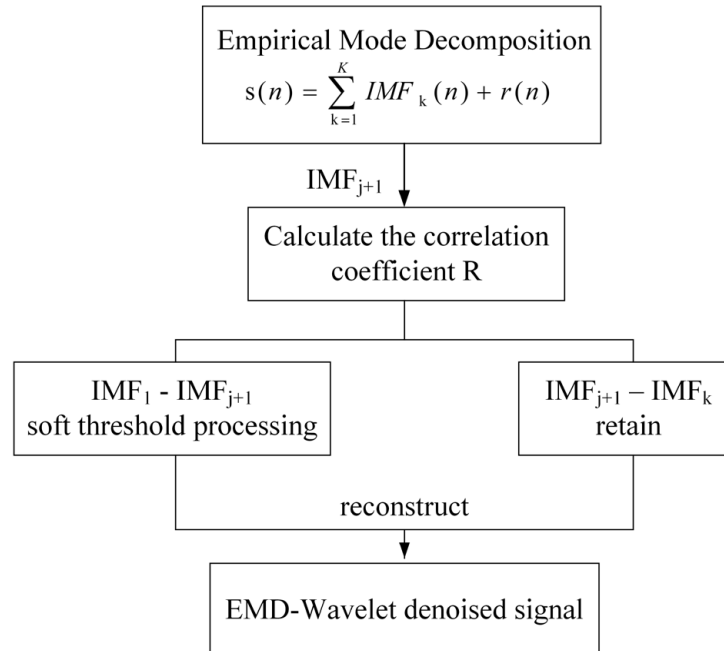


Figure 8. The flow chart of EMD-Wavelet threshold denoising.

Table 1 lists the calculated IMF component correlation coefficients of each component signal. In this table, IMF 4, IMF 4 and IMF 3 are the transition components of H_x , H_y , and H_z after EMD decomposition.

Table 1. Cross-correlation coefficient of IMF components of each magnetic field component signal.

| | IMF 1 | IMF 2 | IMF 3 | IMF 4 | IMF 5 | IMF 6 | IMF 7 | IMF 8 | IMF 9 |
|-------|--------|---------|---------|---------|---------|--------|---------|---------|--------|
| H_x | 0.0172 | −0.0048 | −0.0192 | 0.0072 | 0.3519 | 0.4450 | −0.1817 | −0.0871 | 0.6599 |
| H_y | 0.0099 | 0.0131 | −0.0020 | 0.3681 | 0.8336 | 0.0678 | 0.6418 | — | — |
| H_z | 0.0943 | 0.0366 | 0.0968 | −0.0191 | −0.0107 | 0.4830 | 0.6406 | 0.8038 | 0.7388 |

Figure 9 shows the magnetic signal and gradient value after the EMD-wavelet threshold denoising. It can be seen that EMD-wavelet threshold denoising eliminates the unwanted noise while retaining the useful signal relatively well. The gradient curve is generally flat, and the defect characteristics are obvious.

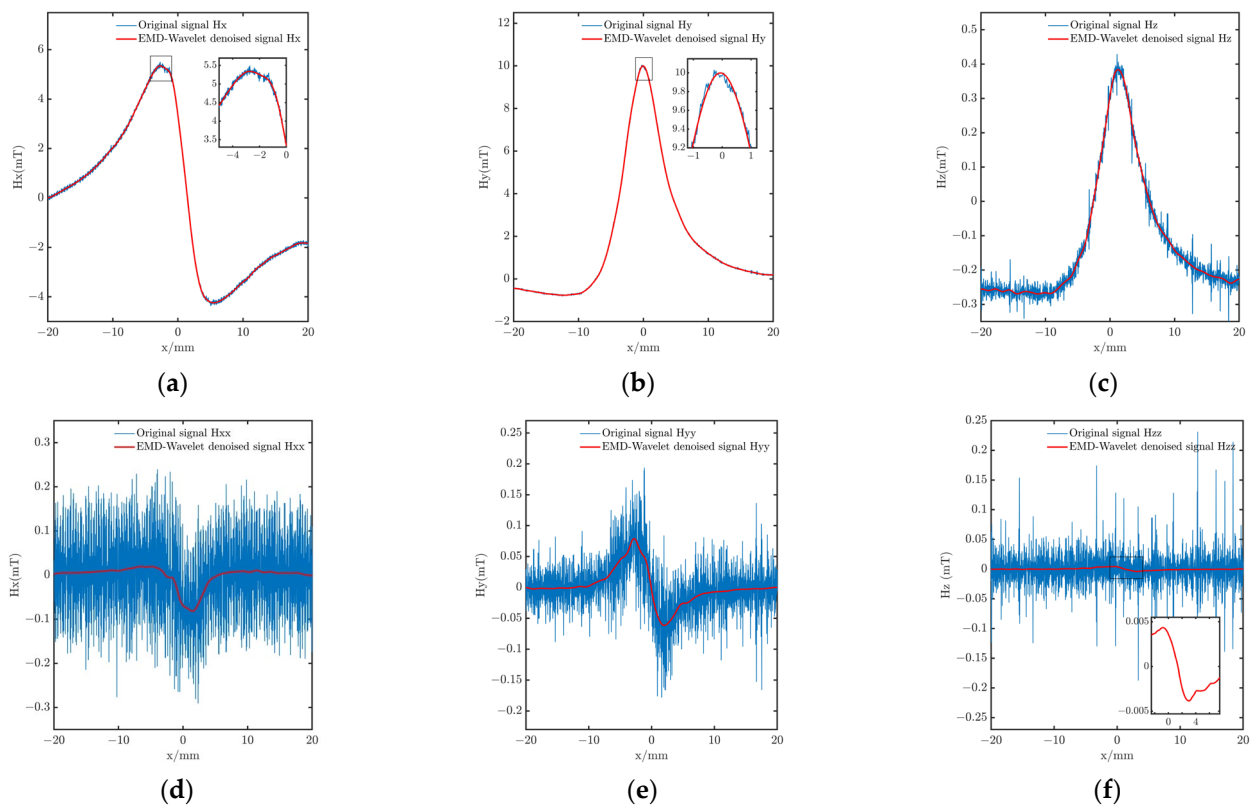


Figure 9. Comparison of EMD-wavelet threshold denoising effects. (a) Comparison of normal component signals. (b) Comparison of tangential component signals. (c) Comparison of horizontal component signals. (d) Comparison of gradient values of normal component signal. (e) Comparison of gradient values of tangential component signal. (f) Comparison of gradient values of horizontal component signal.

3.4. Other Denoising Methods

In addition to wavelet threshold denoising and EMD denoising, the common signal denoising methods also include EEMD, CEEMD, LMD, VMD, EWT and so on. EEMD adds evenly distributed white noise several times during decomposition to cover up the noise in the original signal, which results in a more accurate envelope to avoid modal mixing. The more the ensemble number for EEMD, the better the denoising effect. However, the added white noise will remain after the average processing, and the noise cannot be ignored after reconstruction. CEEMD is improved from EEMD. The added auxiliary noise of CEEMD is a pair of positive and negative white noise with opposite numbers, and there is no redundant auxiliary noise after reconstruction.

LMD can also solve the endpoint effect and mode mixing problem of EMD. According to the envelope characteristics of the signal, adaptive decomposition is carried out. The

decomposed components are product functions, PF, and each product function is obtained by multiplying the envelope function by the pure frequency modulation function.

The VMD method is a non-recursive variational mode signal decomposition method. Its overall framework is a variational problem, which mainly includes the construction and solution of the variational problem. The variational problem is to find the minimum value of the sum of the bandwidth of the center frequency of each modal component, where the intrinsic modal component is defined as the component modal function of amplitude modulation and frequency modulation.

The EWT method combines the adaptive decomposition concept of the EMD method and the tight support framework of the wavelet transform. EWT divides the Fourier spectrum of the signal into continuous intervals, then constructs wavelet filter banks in each interval for filtering, and finally obtains a set of amplitude and frequency-modulated components by signal reconstruction.

The obtained signals are denoised by the above denoising methods, and the results are shown in Figure 10.

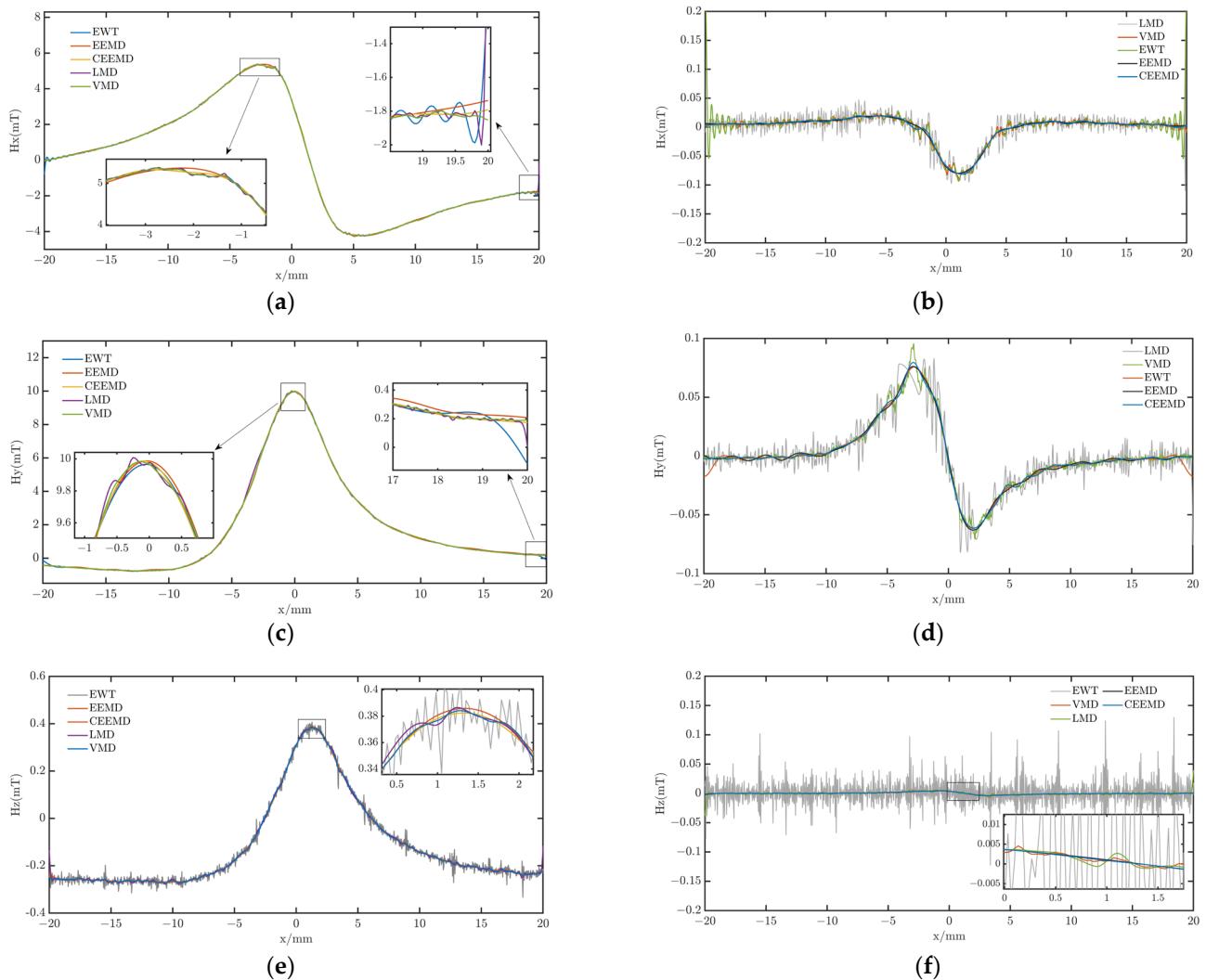


Figure 10. Comparison of signal processing methods. (a) Comparison of normal component signals. (b) Comparison of gradient values of normal component signal. (c) Comparison of tangential component signals. (d) Comparison of gradient values of tangential component signal. (e) Comparison of horizontal component signals. (f) Comparison of gradient values of horizontal component signal.

In Figure 10a,c,e are the denoising effects of the magnetic component signals, and Figure 10b,d,f shows the denoising effects of the gradient signals of magnetic component signals. For the component signals H_x , H_y , and H_z , the denoising results at the peak and the endpoint are greatly different. The denoising effects of LMD, VMD and EWT are not as good as EEMD and CEEMD. The feature value of the defect cannot be obtained, and the location of the defect cannot be judged. The denoising effect of the gradient signal is not as good as that of the component signal, especially the denoising effect of LMD and EWT is not good, which still contains great noise. Figure 10 shows that EEMD and CEEMD are more suitable for denoising enhanced magnetic memory testing signals.

4. Results and Discussion

In order to better compare the signal processing effects of these denoising methods, calculate the SNR of the denoised signal according to Formula (1). The results are shown in Table 2.

Table 2. SNR of different signal processing methods.

| | Normal | Tangential | Horizontal |
|---------------------------------|---------|------------|------------|
| Original Signal | 34.0709 | 40.9030 | 20.6750 |
| Wavelet Threshold Denoising | 51.3965 | 51.2075 | 46.4024 |
| EMD Denoising | 48.5284 | 50.2865 | 53.2229 |
| EMD-wavelet Threshold Denoising | 50.7740 | 53.2229 | 43.6320 |
| EEMD | 42.6955 | 42.4398 | 63.9530 |
| CEEMD | 33.3354 | 30.7251 | 54.9326 |
| LMD | 34.2921 | 36.1620 | 52.2414 |
| VMD | 46.1012 | 47.8602 | 63.1315 |
| EWT | 36.2822 | 40.5297 | 45.8342 |

From Table 2, it can be seen that the denoising effect of wavelet threshold de-noising, EMD-wavelet threshold denoising and EEMD are excellent in the nine de-noising methods. For the normal component signal, the wavelet threshold denoising has the largest SNR at 51.3965; for the tangential component signal, EMD-wavelet threshold denoising has the largest SNR at 53.2229; for the horizontal component signal, EEMD denoising has the largest SNR at 63.9530. The comparative analysis of the denoising effects of these three signal-processing methods is illustrated in Figure 11. The signal curves obtained by the three processing methods, which can reflect the defect characteristics, are very gentle but slightly different.

The proposed improved method EMD-Wavelet threshold denoising has improved the noise reduction effect of tangential component signal to some extent, but the improvement is not significant. For the normal component signal and the horizontal component signal, the proposed method is not as good as Wavelet threshold denoising; therefore, the applicability needs to be improved in future research.

The wavelet threshold denoising method is used to process the signals of 40 paths in the scanning zone, and then the gradient values of the normal component signal and the tangential component signal are plotted in Figure 12.

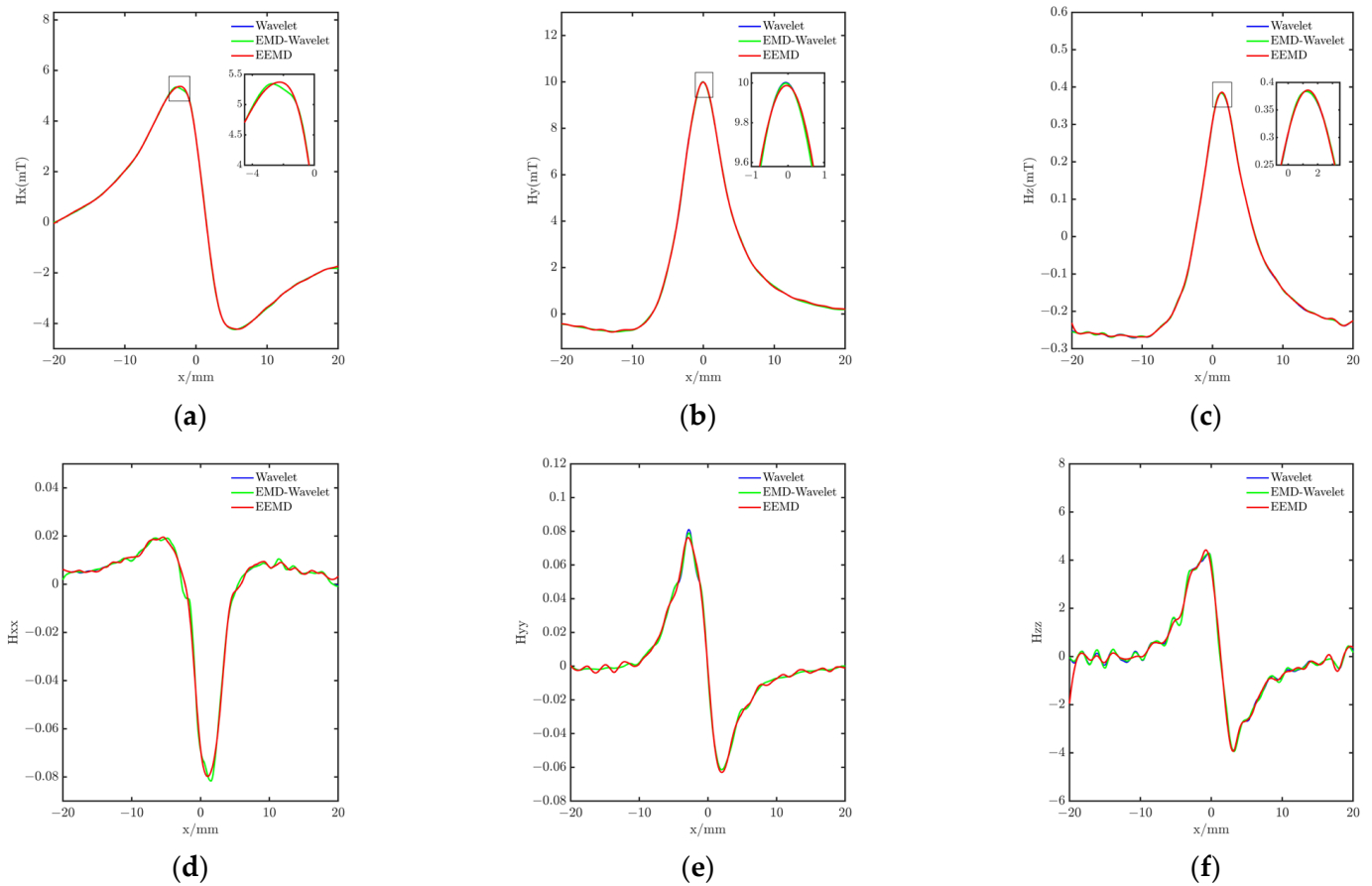


Figure 11. Comparison of three signal processing methods. (a) Comparison of normal component signals. (b) Comparison of tangential component signals. (c) Comparison of horizontal component signals. (d) Comparison of gradient values of normal component signal. (e) Comparison of gradient values of tangential component signal. (f) Comparison of gradient values of horizontal component signal.

It can be seen from Figure 12 that the signal after denoising can generally illustrate the contour characteristics of the defect. The peak value of the normal component H_x on the left side indicates the left boundary of the defect, while the valley value on the right side indicates the right boundary of the defect. The tangential component H_y has a peak at the center of the defect. The horizontal component H_z has a valley at the upper left and lower right corners of the defect. It also has a peak at the lower left and upper right corners of the defect. The normal component gradient H_{xx} has a valley value in the central region, indicating the center of the defect. The tangential component gradient H_{yy} has a peak at the left boundary of the defect and a valley at the right boundary of the defect. The horizontal component gradient H_{zz} has a peak on the upper boundary of the defect and a valley on the lower boundary of the defect.

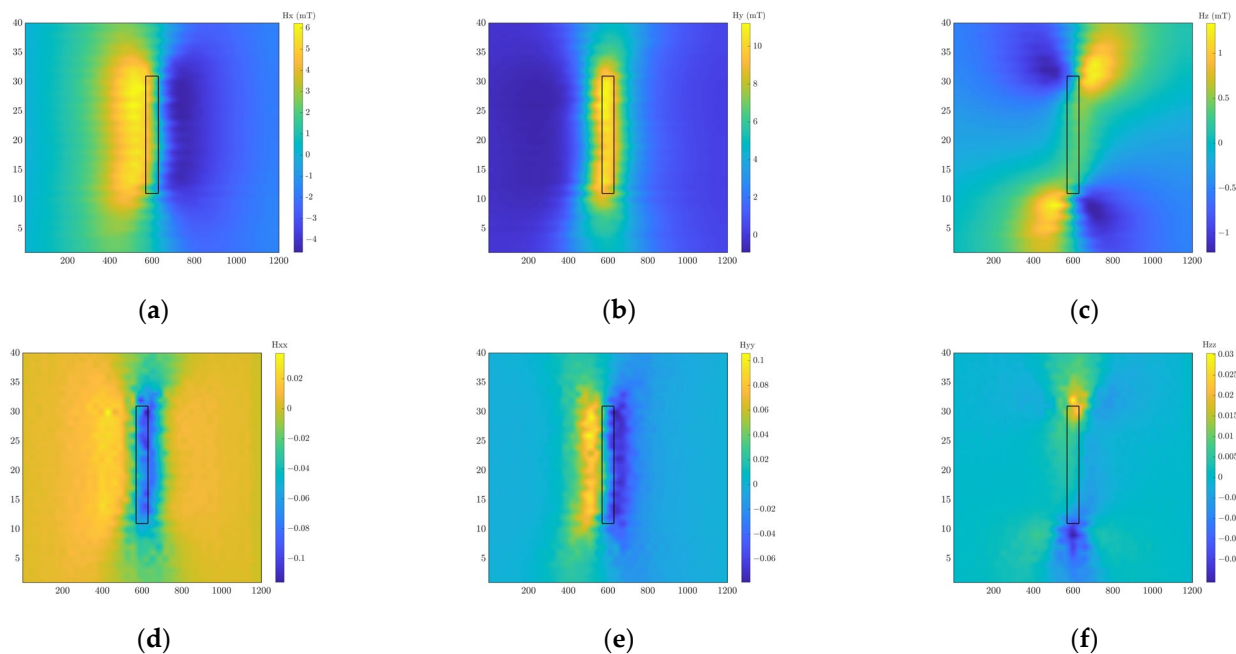


Figure 12. Two-dimensional distribution of defect characteristics. (a) Normal component signals. (b) Tangential component signals. (c) Horizontal component signals. (d) Gradient value of normal component signals. (e) Gradient value of tangential component signals. (f) Gradient value of horizontal component signals.

5. Conclusions

The metal magnetic memory testing signal is weak and is most likely to be affected by interrupting external factors. In order to resolve such problems, this paper adopts the enhanced metal magnetic memory testing method. Firstly, the SNR of the detected signal is improved by gradually strengthening the excitation magnetic field intensity. Then the denoising effects of different signal denoising methods on the detection signal and its gradient value are compared and analyzed. The findings are as follows.

1. Compared with the traditional metal magnetic memory testing method, the enhanced metal magnetic memory testing method can increase the possibility of detecting the signal and enhance the SNR of each component of the detected signal by accurately strengthening the excitation magnetic field. But the enhanced method cannot enhance the SNR of each component of the gradient signal significantly;
2. Among numerous signal processing methods, wavelet threshold, EMD and its improved methods are more applicable in the denoising of enhanced metal magnetic memory testing signals. Taking the signal curve and SNR after denoising into consideration, wavelet threshold denoising, EMD-wavelet threshold denoising and EEMD denoising all have good denoising effects, and the denoising results to the same signal are analogous. It is necessary to determine the best denoising method according to the specific signal.

Author Contributions: Conceptualization, X.L. and L.W.; Methodology, X.L. and L.W.; Validation, L.W.; Formal Analysis, L.W. and S.C.; Data Curation, L.W. and S.C.; Writing—Original Draft Preparation, L.W. and Q.X.; Writing—Review & Editing, X.L., H.Y. and J.Z.; Project Administration, X.L.; Funding Acquisition, X.L. All authors have read and agreed to the published version of the manuscript.

Funding: This research was funded by Sichuan Science and Technology Program under Grants 2021YFS0305, 2022ZYD0020, and 2022NSFSC0450 and The Chengdu Technological Innovation R&D Project under Grant 2022-YF05-00861-SN.

Data Availability Statement: There is no associate data in this study.

Acknowledgments: I would like to sincerely acknowledge the helpful financial support from the Sichuan Science and Technology Program and thanks for the financial support from The Chengdu Technological Innovation R&D Project. In addition, I wish to thank all the members of our team for their contributions to this task.

Conflicts of Interest: The authors declare no conflict of interest.

References

1. Shi, P.; Su, S.; Chen, Z. Overview of researches on the nondestructive testing method of metal magnetic memory: Status and challenges. *J. Nondestruct. Eval.* **2020**, *39*, 43. [[CrossRef](#)]
2. Luo, X.; Wang, L.; Lv, L.; Cao, S.; Dong, X.; Zhao, J. Forward model of metal magnetic memory testing based on equivalent surface magnetic charge theory. *Acta Phys. Sin.* **2022**, *71*, 103–119. [[CrossRef](#)]
3. Qiu, Z.; Hong, L.; Yao, Z.; Yang, J.; Zhang, R. Early prediction of fracturing failure for bolted joints based on enhanced metal magnetic memory. *Insight* **2019**, *61*, 603–607. [[CrossRef](#)]
4. Li, B.; Zhang, J.; Chen, Q. Theoretical and experimental research on wire rope magnetic memory testing under weak magnetic excitation. *Insight* **2022**, *64*, 91–98. [[CrossRef](#)]
5. Wang, C.; Zhu, H.; Xu, C.; Yu, W. Application of adaptive wavelet threshold de-noising in metal magnetic memory signal processing. *J. Syst. Eng. Electron.* **2012**, *34*, 1555–1559.
6. Jian, Q. Study on the Quantification of Tubing Defects Based on Magnetic Flux Leakage Testing. Master's Thesis, Southwest Petroleum University, Chengdu, China, 2015.
7. Zhu, S. Early Fault Detection of High-Speed Train Wheel Set Based on Metal Magnetic Memory Effect. Master's Thesis, Jiangsu University, Zhenjiang, China, 2019.
8. Wen, H. Research on Deformation Analysis Model Based on Wavelet Transform Theory. Master's Thesis, Wuhan University, Wuhan, China, 2004.
9. Yi, F.; Li, Z.; Su, Y.; Wang, P.; Wu, H. Denoising algorithm for metal magnetic memory signals of oil pipeline based on improved wavelet threshold. *Acta Pet. Sin.* **2009**, *30*, 141–144.
10. Huang, N.E.; Shen, Z.; Long, S.R.; Wu, M.C.; Shih, H.H.; Zheng, Q.; Yen, N.C.; Tung, C.C.; Liu, H.H. The empirical mode decomposition and the Hilbert spectrum for nonlinear and non-stationary time series analysis. *Proc. R. Soc. Lond. Ser. A* **1998**, *454*, 903–995. [[CrossRef](#)]
11. Huang, N.E.; Shen, Z.; Long, S.R. A new view of nonlinear water waves: The Hilbert spectrum. *Annu. Rev. Fluid Mech.* **1999**, *31*, 417–457. [[CrossRef](#)]
12. Leng, J.; Xu, M.; Zhang, J. Application of empirical mode decomposition in early diagnosis of magnetic memory signal. *J. Cent. South Univ. Technol.* **2010**, *17*, 549–553. [[CrossRef](#)]
13. Wu, Z.; Schneider, E.K.; Kirtman, B.P.; Sarachik, E.S.; Huang, N.E.; Tucker, C.J. The Modulated Annual Cycle: An Alternative Reference Frame for Climate Anomalies. *Clim. Dyn.* **2008**, *31*, 823–841. [[CrossRef](#)]
14. Li, Z. The Research of Metal Magnetic Memory Technology in the Flaw Identification of Mining Steel Rope. Master's Thesis, Taiyuan University of Technology, Taiyuan, China, 2016.
15. Ye, H. Research on Mine Wire Rope Defect Detection System Based on Three Axis Magnetic. Master's Thesis, Taiyuan University of Technology, Taiyuan, China, 2018.
16. Zheng, H.; Wang, C.; Pan, S.; Gao, W. Research on noise reduction method of magnetic memory signal based on EEMD and layered threshold. *Chin. J. Eng. Des.* **2020**, *27*, 433–440.
17. Yeh, J.R.; Shieh, J.S.; Huang, N.E. Complementary ensemble empirical mode decomposition: A novel noise enhanced data analysis method. *Adv. Adapt. Data Anal.* **2010**, *2*, 135–156. [[CrossRef](#)]
18. Gu, J.; Peng, Y. An improved complementary ensemble empirical mode decomposition method and its application in rolling bearing fault diagnosis. *Digit. Signal Process.* **2021**, *113*, 103050. [[CrossRef](#)]
19. Wang, C. Research on Defect Diagnosis Method of Natural Gas Pipeline Based on CEEMD. Master's Thesis, China University of Petroleum, Beijing, China, 2020.
20. Ju, H.; Wang, X.; Zhao, Y. Research on defect signal extraction algorithm of steel pipeline based on improved VMD. *Chin. Meas. Test.* **2020**, *46*, 100–107.
21. Chen, Y.; Gao, P.; He, T.; Liu, X.D. Roller bearing comprehensive fault diagnosis based on LMD. *J. Vib. Shock* **2012**, *31*, 73–78.
22. Lu, C.; Xia, F. Microseismic noise reduction based on EWT and Meyer adaptive threshold. *Prog. Geophys.* **2020**, *35*, 1010–1016.
23. Ning, Y.; Wei, Z.; Zhou, J. Fault diagnosis of low-speed heavy-duty bearings of mixers based on improved EMD and wavelet threshold. *Noise Vib. World* **2020**, *40*, 134–139.

Disclaimer/Publisher's Note: The statements, opinions and data contained in all publications are solely those of the individual author(s) and contributor(s) and not of MDPI and/or the editor(s). MDPI and/or the editor(s) disclaim responsibility for any injury to people or property resulting from any ideas, methods, instructions or products referred to in the content.